Traditional vs Numerical Methods to Estimate Pressures and Strains in Pond Geomembrane Bubbles

Thiel, Richard
President, Thiel Engineering, USA (richard@rthiel.com)

Eldesouky, Hesham
Post-doctoral fellow, Dept. of Civil Engrg., Queen's U., CANADA (hesham.eldesouky@queensu.ca)

Brachman, Richard
Professor, Geo-Engineering Center, Queen's U., CANADA (richard.brachman@queensu.ca)

ABSTRACT: Ponds constructed with exposed geomembranes are susceptible to geomembrane uplift caused by trapped gases below the liner. Being able to model and understand the pressures and strains in geomembrane bubbles occurring in ponds can aid designers and operators to manage and avoid these common nuisance situations that often result in rupture of the geomembrane. Thiel (2016) provided an approximate mathematical model based on engineering equations for static equilibrium that utilized iterative calculations to analyze the shape, internal pressure, stresses, and strains in a geomembrane gas-filled bubble whose pressure is caused by the surrounding impounded fluid. While that model was deduced based on engineering principles, and its solutions appeared to correlate with field observations, the calculated results clearly contained unrealistic strain discontinuities, and there were no detailed field or laboratory studies performed against which the results could be compared. Recent finite element analysis (FEA) modeling of this problem was performed by Queen's University out of Kingston, Ontario, Canada. The results of the FEA modeling were found to compare relatively closely to the approximate static-equilibrium model, and also provided a continuity in the strain gradient along the bubble surface that continued into the surrounding free-field geomembrane on the pond floor. The FEA results were able to show the changes in bubble pressure and strain distribution depending on the assumed interface friction between the geomembrane and the pond subgrade material below the geomembrane, which is a variable that was not able to be considered with the approximate equilibrium model. A comparison of the results indicate that the approximate static-equilibrium model likely provides conservative results for practitioners who do not have access to FEA modeling. The FEA modeling will prove useful for performing sensitivity analyses affecting the bubble pressure and strain distribution such as the bubble size, water depth, geomembrane thickness, geomembrane modulus, and interface friction with the pond bottom.

Keywords: pond, geomembrane, strain, bubble, whale

1 INTRODUCTION

There is a substantial legacy of literature devoted to the design, construction, and operation of geomembrane-lined ponds and reservoirs going back to the early 1980s. Even with this long history there continue to be problems and failures with lined ponds. One of the problems continuing to plague the industry is that of uplifted geomembrane gas bubbles, also called "whales" or "hippos", which do not go away in ponds that have an exposed geomembrane. Gas bubbles

trapped under the geomembrane have been reported as a problem in the literature for over 30 years (e.g. Giroud, 1983). A photo of typical pond bubbles is show below in Figure 1.

Figure 1. Bubbles in pond with 1.5 mm HDPE geomembrane on verge of bursting.

Bubbles in exposed pond geomembranes result from a certain volume of trapped air (or gas) below the geomembrane. As the pond is filled with water (or other liquid) the trapped air becomes pressurized and forms a 'bubble' whose shape and pressure are a function of, among other things, the volume of trapped air and the depth of the liquid. The volume of trapped air is created by the field conditions, which are very difficult, if not impossible, to predict. The trapped air or gases can come from several sources (Giroud 1983) including air trapped below the newly-deployed geomembrane wrinkles (Wallace et al. 2006), which is investigated in this study, air pushed up through the subgrade soils by rising ground water (Cao et al. 2015), gases generated by decomposing organics in the subgrade, gas generated by chemical reactions between leaking liquid and subgrade soils, or biologically active liquid trapped below the geomembrane (Peggs 2006). Experience has shown that bubbles have commonly manifested in sizes ranging from 1-30 meters in diameter, and maybe even outside of those limits.

Bubbles are deleterious for ponds for several reasons including: pressures in the bubbles (although relatively low) can cause strains in the geomembranes that threaten the integrity of the geomembrane and can cause it to burst (Thiel 2016); bubbles lift the geomembrane off the pond bottom and, if there is a leak in the geomembrane, can result in massive flooding below the primary geomembrane thus nullifying much or all of the intended benefit of the geomembrane; the bubble(s) may occupy a significant volume of the pond and thus reduce the value of the pond's holding capacity; the exposed bubble is susceptible to damage through physical exposure and documented instances of cyclic stress cracking due to wind, waves, and thermal cycles (Marta and Armstrong, 2020; Peggs 2012).

When bubbles occur, it is important for pond operators to lower liquid levels and attempt to move the bubbles to pond perimeters where they can be vented (Thiel 2016b). Sloped pond bottoms with a minimum of obstacles are advantageous in this regard.

The research presented in this paper is valuable to pond designers and operators. There have been many instances of bubbles occurring in ponds, resulting in unhappy owners and questions of allocation of remediation costs between owners, designers, contractors, and installers. Understanding of the mechanisms and sensitivities of exposed pond liners, and the susceptibility to bubble formation, can help avoid these situations, or help unravel why they occurred to help resolve questions of responsibility. Understanding the sensitivity of the pressures and strains in pond bubbles will allow designers to appropriately apply the necessary design principles to address these issues, and operators to manage them once they occur.

2 PREVIOUS EVALUATIONS OF POND BUBBLES

To the authors' knowledge, there have been only two previous attempts to model the realistic shapes, stresses, and strains in a geomembrane bubble. These were made by Guo et al. (2016) and Thiel (2016a). The two approaches were developed completely independent of each other. Both methods were based on the principle of static equilibrium. Guo et al. (2016) describes an analysis by summing the forces of the bubble pressure, geomembrane tension, and hydrostatic pressures in the horizontal direction, assuming a constant tension throughout the bubble that continues into its tangent with the subgrade. Thiel (2016a) provided analytical methods to predict the size, shape and pressure of gas bubbles by summing the forces in the vertical direction with the assumption that the portion of the bubble above the point of inflection was circular, and the portion below the point of inflection was a clothoidal spiral, with the resulting stresses and strains having quantum changes between different segments of the bubble and ending at the tangent with the subgrade. Neither method was able to account for the influence of the friction between the geomembrane and the subgrade around the perimeter of the bubble, nor for a realistic continuum of strain variations into its tangential merge with the subgrade. Both methods relied on an iterative calculation approach to reach a solution. The details of the calculations were provided by Thiel (2016a) in a manner that could be replicated in a spreadsheet, whereas the details provided by Guo et al. (2016) referenced a computer programming scheme employing a 'Complex Method' to search for the unknown parameters. The intent of both models was to evaluate a 3D axisymmetric bubble. Guo et al. (2016) assumed the radial forces in the bubble are constant along its profile, and the developed radial elongation, or strain, is independent from tangential forces. The basis of the strain calculation in Thiel model assumes constant strain, along the upper portion of the bubble, driven from axisymmetric conditions as in multiaxial testing (ASTM D5617). The goal of this study is to compare these traditional methods with a numerical analysis approach of the bubble problem which takes in account the change in strain, and radial forces, along the bubble.

3 FINITE ELEMENT ANALYSIS (FEA)

3.1 *Bubble formation*

This study investigates the bubble formation due to entrapped air under a geomembrane wrinkle. Wrinkles, formed during construction, entrap air with an atmospheric absolute pressure P_a and an initial volume V_o below the geomembrane. As the water pressure builds on the geomembrane, the volume of wrinkle, hence the air volume, V, decreases and air gauge pressure P (absolute air pressure = $P + P_a$) increases following the ideal gas law:

$$V_o\, P_a = V\,(P + P_a) \qquad [1]$$

The air in the wrinkle creates the axisymmetric bubble shape due to the surrounding pond liquid pressure, creating a net uplift pressure on the geomembrane bubble. In addition, the bubble can grow at that location if it merges with nearby bubbles to form a bigger bubble.

3.2 *FEA model*

The bubble formation as it develops from an assumed quantity of air trapped below a wrinkle was modeled using the finite element package ABAQUS (2017). For model simplicity, one axisymmetric conical wrinkle entrapping an initial volume V_o of 654.5 m^3 of air under atmospheric absolute pressure, P_a = 101.3 kPa, was modeled, Figure 2a. The pressures used in the model and reported in the paper are gauge pressure, and hence, the initial air gauge pressure implemented in the model is zero. More than three hundred quadratic shell elements were used

for modelling a 1.5 mm linear elastic geomembrane with an elastic modulus of 150 MPa (stiffness of 225 kN/m) and Poisson's ratio of 0.46 overlying a rigid subgrade. The subgrade was fixed in both vertical and radial directions (no vertical or radial displacements $u_z = u_r = 0$) while no radial displacement ($u_r = 0$) was imposed on the geomembrane at a radius of 50 m, simulating the half distance between two adjacent bubbles. Three interface friction angles δ between the geomembrane and the subgrade were examined, 0°, 10° and 20°. A hydrostatic water gauge pressure P_w was applied on the top surface of the geomembrane which increases linearly with water depth;

$$P_w = (H_w - z)\,\gamma_w \qquad [2]$$

where H_w = water height [m]; z = the vertical coordinate of the point where the pressure is calculated at [m]; and γ_w = unit weight of water (9.81 kN/m^3).

The simulation involved high degrees of nonlinearity in both geometry and loading. The water pressure was applied in increments in which the water height was changed by $\Delta H \leq 2$ cm increments. At each increment, the water pressure on the geomembrane was calculated using equation [2] and zero water pressure was applied on the geomembrane portions above the water level H_w. Under the water pressure increment, the geomembrane deforms, reducing the air volume and resulting in an increase in air gauge pressure, equation [1], on the bottom surface of the geomembrane, Figure 2b. Before proceeding to the next increment, the final deformed shape of the geomembrane was calculated by iterating between equation [1], [2] and a stiffness matrix until a force equilibrium with an error less than 0.5% was achieved. The increment size was reduced by a factor of 0.25 if the equilibrium error was not achieved within 35 iterations. A final water height of 5 m was modeled in more than 250 increments.

4 FEA RESULTS

Air pressure increases as water depth increases resulting in higher (taller) bubbles but slightly smaller in volume for a fixed initial air volume, as indicated in Figure 3 which compares the bubble shape for two different water heights. The bubble tends to take a bell shape due to the air pressure inside resisting the pressure of the water surrounding the bubble.

The strain, ε, in the geomembrane varies along the bubble profile depending on the water level, H_w, with a gradual reduction to zero after some horizontal distance, depending on the interface friction angle, δ, from the geomembrane-subgrade first contact point, Figure 3. At low water levels, the FEA calculated the maximum strain below the water line, Figure 3a. However, as the water level goes higher, the strain in upper portion of the bubble increases rapidly and becomes greater towards the pole (top) of the bubble, Figure 3b.

The maximum strain value, ε, in the geomembrane increased with water depth, and a higher interface friction angle δ resulted in higher maximum strains, Figure 4. An interface friction angle δ of 20° showed a maximum strain of 31% at a water level, H_w, of 5 m, compared to 27% for smooth interface, $\delta = 0°$. The clamping effect imposed by subgrade friction reduces the geomembrane free length that can deform, and hence, increases strain.

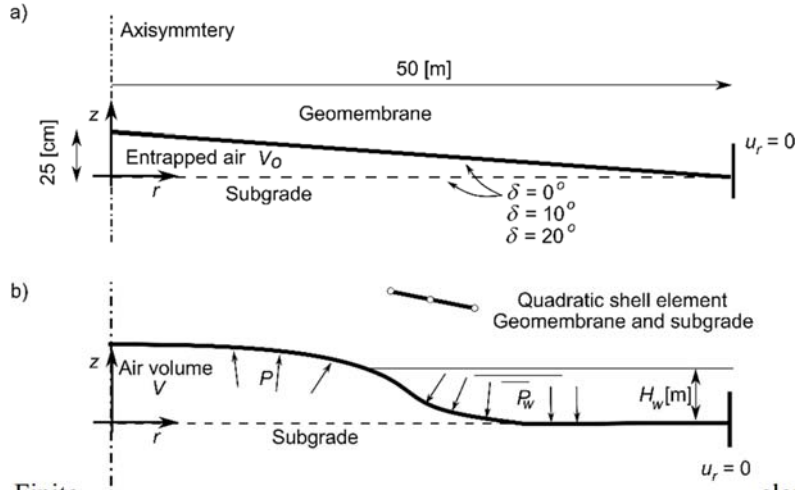

Figure 2. Finite element model. a) undeformed shape and b) deformed shape and loads.

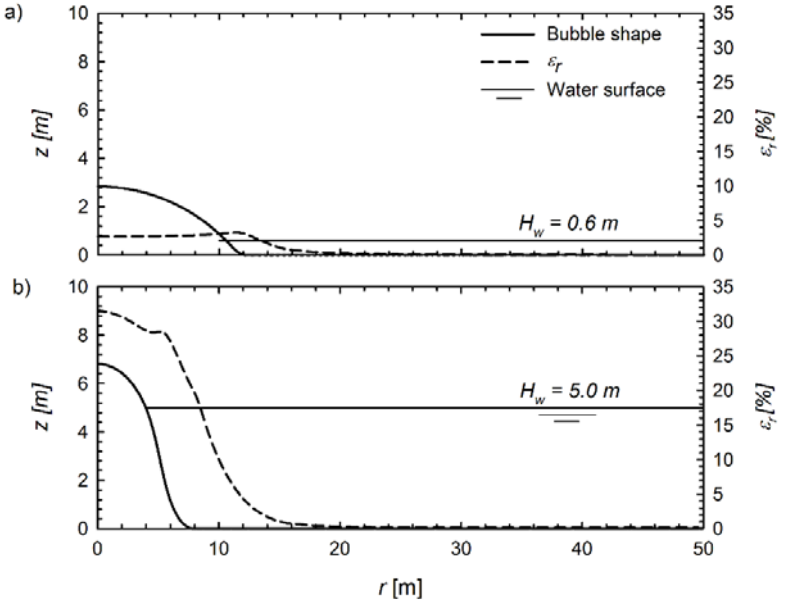

Figure 3. Bubble shapes and strain for various water heights (δ= 20°). a) H_w =0.6 m and b) H_w = 5.0 m.

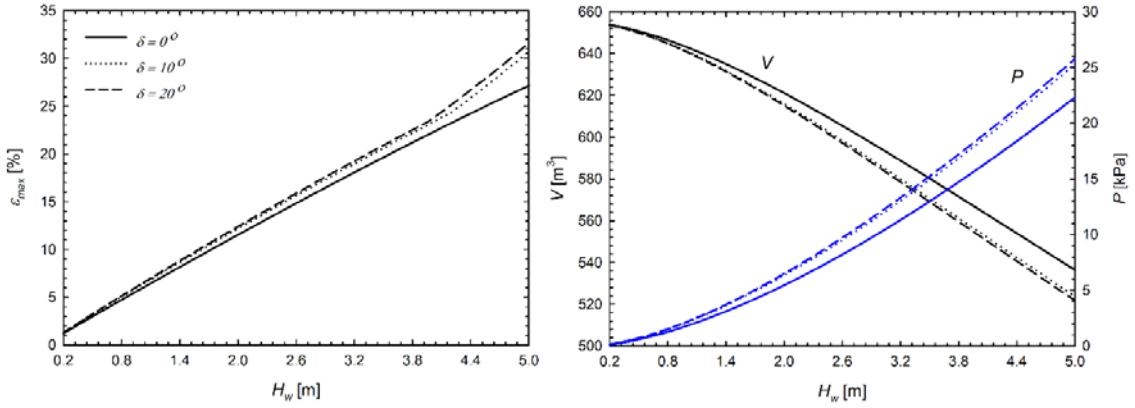

Figure 4. Geomembrane maximum strain, air volume and pressure versus water height for various interface friction angle for an assumed bubble initial volume of 654 m^3.

5 FEA RESULTS VERSUS STATIC EQUILIBRIUM APPROACH

Comparing the bubble shapes calculated by the FEA with the approximate static equilibrium approach developed by Thiel (2016a) indicated very close agreement assuming the same bubble height (H_b = 3.04 m), bubble radius (r_b = 11.88 m), and depth of water (H_w = 0.60 m). The agreement was closest when the FEA approach assumed the interface friction between the geomembrane and the subgrade to be 20° (the Thiel method assumes zero). A comparison of the results for a single case are presented in Figure 5. In addition to the predicted shapes of the bubbles being very close, the following quantitative comparison of results of calculated pressures, volumes, and strains were also obtained:

- The calculated internal bubble pressure, P, by the approximate Thiel (2016a) approach was 8.4% higher than the FEA method (1.03 vs 0.95 kPa).
- The calculated volume of the bubble, V, by the approximate Thiel (2016a) approach was 5% lower than the FEA method (612 vs 648 m^3).
- The strain estimated by the Thiel method for the zone above the water line was 3.95%, while FEA results show the strain varying from 3.0% at the pole, to 3.7% at the water line.
- Thus, the "simplistic spreadsheet model" is more conservative than then FEA model, but still relatively accurate, at least for that example.

It is relatively remarkable that the simplified spreadsheet approach compared so favorably to the FEA method, given that the two methods were based on completely unique and independent approaches. Whereas the simplified spreadsheet method could only assume average strains in discrete zones of the bubble, with unrealistic step functions in the strain estimates along the bubble profile, and unrealistic values of strains in certain portions of the bubble, the FEA method is able to (a) take into account bottom friction of the liner with the subgrade, and (b) to describe a continuum of strain values and strain gradients throughout the bubble profile and extending into the free-field geomembrane surrounding the bubble. This amazing correspondence between the two methods to describe the shape, pressure, and strains in geomembrane bubbles provides a validation of their relative accuracy, which is also corroborated by field observations. Furthermore, the potentially powerful ability of the FEA method to explore many nuances in a more precise manner allows sensitivity analyses to be expeditiously carried out.

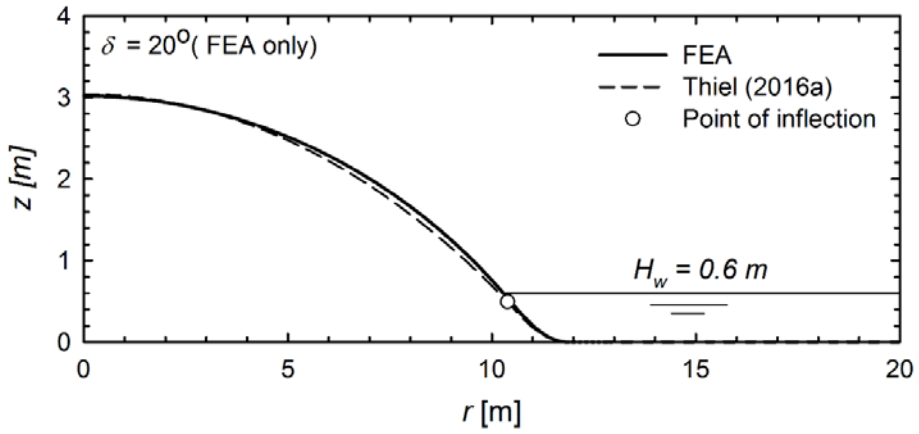

Figure 5. Comparison of Thiel (2016a) method and FEA for predicting bubble shape. Note that FEA assumed $\delta = 20°$, whereas the Thiel method assumes $\delta = 0°$.

Another example comparison was made between the the Guo et al. (2016), Thiel (2016a), and FEA methods. The results for one particular set of assumptions taken from the Guo et al. paper were attempted to be replicated by the other two methods. A summary of the results is presented in the table below.

Table 1. Comparison of bubble parameters for one particular case using 3 different methods

Bubble parameter	Results using Guo et al. (2016) method[(1)] / [***difference compared to FEA***]	Results using Thiel (2016a) method / [***difference compared to FEA***]	Results using FEA method
bubble radius, r_b, from top of bubble to tangent with subgrade (m)	8.0 [***3.2%***]	8.3 [***7.4%***]	7.75
bubble height, H_b, from subgrade to top of bubble (m)	3.70 [***2.2%***]	3.62 [***0%***]	3.62
depth of water, H_w (m)	2.0 [***0%***]	2.0 [***0%***]	2.0
volume of the bubble, V (m^3)	286 (est.) [***2.0%***]	236 [***-16%***]	280.5
internal bubble pressure, P (kPa)	5.1 [***-31%***]	7.9 [***6.8%***]	7.4
geomembrane stiffness, Et (kN/m)	300 [***0%***]	300 [***0%***]	300
calculated strain, ε, near the water line (%)	12.7 (est.) [***43%***]	10.1 [***13%***]	8.9
friction, δ, between subgrade and geomembrane	0° [***0%***]	0° [***0%***]	0°

(1) The values for the Guo et al. (2016) method are estimated from the graphs and other information presented in their paper.

In attempting to replicate the Guo et al. results with the Thiel method, the depth of water was held equal at 2.0 m and the geomembrane stiffness for the upper half of the bubble was held at 300 kN/m' to match the Guo et al. values, and the other parameters were varied manually to achieve results as close as possible to the Guo et al. (2016) results. The FEA model was set up by holding the same water depth, geomembrane stiffness, and initial air volume (300 m^3) as the Guo et al. model, and allowing the air volume to adjust with the calculated pressure as was done in the Guo et al. model. The resulting bubble radii and bubble heights were similar for all three models. The largest differences were for the calculated pressures and strains, where the Guo et al. pressures were substantially lower, and the strains substantially higher, than the other two models. The lower calculated pressure in the Guo et al. (2016) model is suspected to be due to the simplified constant force radial assumption. The Thiel model was found to be conservative (i.e. higher values) relative to the FEA model with regard to both the estimated bubble pressure and strain.

6 CONCLUSIONS

Using two completely separate and different approaches, the results of the FEA modeling were found to compare relatively closely to the approximate Thiel (2016a) static-equilibrium model in assessing geomembrane bubble shape, strain, and pressure for a given amount of trapped air volume.

The FEA model provides a continuity in the strain gradient along the bubble surface that continues into the surrounding free-field geomembrane on the pond floor, which is much more realistic than the simplified step-functions of strain regimes assumed by the Thiel (2016a) simplified static model.

The FEA results were able to show the changes in bubble pressure and strain distribution depending on the assumed interface friction between the geomembrane and the pond subgrade material below the geomembrane, which is a variable that was not able to be considered with the approximate equilibrium models.

The FEA was utilized to simulate the bubble formation during pond filling, and the estimated strain corresponding to each water level was calculated. An example was presented showing the maximum strain in the geomembrane liner increased with water height, and theoretically would reach a strain of more than 27% at a water height of 5 m. Clearly this level of strain is dangerous for the geomembrane (it would likely yield and burst), and under the simulated conditions it would be recommended to lower the water level in the pond once bubbles start to develop, and to take measures to vent the bubbles. The attempt to reduce bubble size, hence strain, by increasing water level is not an effective strategy and would result in the opposite of the intended results, at least up until the point the bubble is submerged. One interesting finding from the FEA study is that geomembranes with a lower interface friction angle with the subgrade soil, such as provided by a smooth geomembrane, are predicted to experience less strain due to bubbles than materials with a higher interface friction because of the way that the bubble stresses are able to distribute over a larger area.

Graphs such as the one shown in Figure 4 could be developed for different assumed trapped air volumes. These types of graphs, combined with maximum allowable strains that would be assigned for the type of geomembrane being used at a project operating temperature, could be used to make management decisions regarding pond operations. Ideally the understanding gained from these relationships would also aid designers to implement designs that would avoid such bubbles from ever developing.

The results indicate that the approximate spreadsheet-based static-equilibrium model likely provides conservative results for practitioners who do not have access to FEA modeling. The FEA modeling will prove useful for performing sensitivity analyses. Additional parametric studies of the effects of bubble size (viz. volume), water depth, and interface friction on the predicted bubble pressures and strains for different geomembrane stiffnesses are warranted.

REFERENCES

ABAQUS, 2017. Abaqus/CAE user manual 2017. Dassault Systèmes, Providence, RI, USA.

Cao, X., Yuan, J., He, G., Liu, Y., Yin, Z. (2015) In situ test and analysis method of air bulging under geomembranes in a shallow-lined reservoir. *Geotextiles and Geomembranes*, **43**, No. 3, 24-34.

Giroud, JP (1983) General report on geomembrane lined reservoirs. Seminar on Surface Waterproofing, Session 2 on Reservoirs, Paris (in French).

Guo, W., Chu, J., Zhou, B., and Sun., L. (2016) Analysis of geomembrane whale due to liquid flow through composite liner. *Geotextiles and Geomembranes*, **44**, No. 3, 247-253.

Marta, A. and Armstrong, C. (2020) Brittle stress cracking of HDPE geomembrane caused by localized over heating of fusion wedge welds and whales. *Paper submitted for acceptance to GeoAmericas 2002 to be held in April 2020, Brazil.*

Peggs, I. (2006) The pond edge: geomembrane liners in wastewater treatment ponds: whales, and their prevention. *Land and Water Magazine,* Frontiernet, Volume: 50, Issue: 4.

Peggs, I. (2012) Impact of variable stresses on accelerated stress cracking of HDPE wrinkles. *Proceedings of GeoAmericas 2012, May, Lima, Peru.*

Thiel, R. (2016a) Analysis of stresses and strains in geomembrane gas bubbles that occur in surface impoundments. *Proceedings for Geo-Chicago 2016*, American Society of Civil Engineers, Chicago, Illinois, USA, August 14-18, 2016.

Thiel, R. (2016b) Recommendations for Design of Exposed Geomembrane-Lined Ponds to Control Uplifting Gas Pressures. *Proceedings for Eurogeo6,* International Geosynthetics Society, Ljubljana, Slovenia, September 25-28, 2016.

Wallace, R, Giroud, JP, and Shanks, M. (2006) Impacts of construction practices and reservoir filling on geomembrane uplift. *Proceedings of the 8th International Conference on Geosynthetics*, Yokohama, Japan, Vol. 2, pp. 615-618.